crystals

MDPI

Article

# Morphological and Crystallographic Characterization of Primary Zinc-Rich Crystals in a Ternary Sn-Zn-Bi Alloy under a High Magnetic Field

**Lei Li [1,2], Chunyan Ban [1,2,*], Ruixue Zhang [1,2], Haitao Zhang [1,2], Minghui Cai [2], Yubo Zuo [1,2], Qingfeng Zhu [1,2], Xiangjie Wang [1,2] and Jianzhong Cui [1,2]**

1 Key Laboratory of Electromagnetic Processing of Materials, Ministry of Education, Northeastern University, Shenyang 110819, China; lilei@epm.neu.edu.cn (L.L.); zrx532@163.com (R.Z.); haitao_zhang@epm.neu.edu.cn (H.Z); zuoyubo@epm.neu.edu.cn (Y.Z.); zhuqingfeng@epm.neu.edu.cn (Q.Z.); wangxj@epm.neu.edu.cn (X.W.); jzcui@epm.neu.edu.cn (J.C.)

2 School of Materials Science and Engineering, Northeastern University, Shenyang 110819, China; cmhing@126.com

* Correspondence: bancy@epm.neu.edu.cn; Tel.: +86-24-8368-1895

Academic Editor: Matthias Weil

Received: 3 June 2017; Accepted: 3 July 2017; Published: 6 July 2017

**Abstract:** Due to the unique capacity for structural control, high magnetic fields (HMFs) have been widely applied to the solidification process of alloys. In zinc-based alloys, the primary zinc-rich crystals can be dendritic or needle-like in two dimensions. For the dendritic crystals, their growth pattern and orientation behaviors under HMFs have been investigated. However, the three-dimensional crystallographic growth pattern and the orientation behaviors of the needle-like primary zinc-rich crystals under a high magnetic field have not been studied. In this work, a ternary Sn-Zn-Bi alloy was solidified under different HMFs. The above-mentioned two aspects of the needle-like primary zinc-rich crystals were characterized using the Electron Backscattered Diffraction (EBSD) technique. The results show that the primary zinc-rich crystals are characterized by the plate-shaped faceted growth in three dimensions. They grow in the following manner: spreading rapidly in the {0001} basal plane with a gradual decrease in thickness at the edges. The application of HMFs has no effect on the growth form of the primary zinc-rich crystals, but induces their vertical alignment. Crystallographic analysis indicates that the vertically aligned primary zinc-rich crystals orient preferentially with the *c*-axis perpendicular to the direction of the magnetic field.

**Keywords:** high magnetic field; solidification; zinc-rich crystal; characterization; crystallography; EBSD

## 1. Introduction

Since the last century, great attention has been devoted to the application of a magnetic field to the solidification process of alloys due to its unique capacity for structural control [1–23]. Before the development of superconducting magnets, a conventional magnetic field (usually smaller than 2 T) was the most extensively used in research and practice. Owing to the low intensities, conventional magnetic fields mainly affect the structures of alloys through suppressing or driving the fluids by the induced Lorentz force [1–5]. With the recent development of the superconducting magnet, high magnetic fields (HMFs) (usually larger than 2 T) have become readily available and have been widely introduced in the solidification process of alloys. When compared to the conventional magnetic fields, the HMFs significantly enhance the Lorentz force and the magnetization force (usually negligible in conventional magnetic fields), thereby imposing more abundant effects on the structures of the alloys [6–23]. It has been found that the HMFs could orient and align the structures [13–17], increase the

phase transformation temperature [19], enhance the magnetic coercivities [16], suppress the diffusion of solute elements [21], modify the orientation relationship between the eutectics [22], and change the solid-liquid interface morphologies [23].

Hexagonal close-packed zinc is characterized by large solid-liquid interfacial energy anisotropy [24,25] and magnetocrystalline anisotropy [13,14]. Therefore, it is of fundamental interest to study its growth under HMFs. In other work, it has been shown that the primary zinc-rich crystals in Zn-Al [13] and Zn-Sn [14,26] alloys have a dendritic form (preferentially grow along $\langle 10\bar{1}0 \rangle$ and/or <0001>) and can be preferentially aligned and oriented by HMFs. According to some recent work, the primary zinc-rich crystals in ternary Sn-Zn-Bi solder alloys usually exhibit a needle-like morphology in two dimensions [27]. However, their crystallographic growth pattern in three dimensions has not been addressed. The crystallographic effects of HMFs on such crystals are also not clear. Based on this context, a ternary Sn-12Zn-6Bi alloy (nominal composition: wt %) was solidified under various HMFs in this work. The three-dimensional growth form, the alignments, and the orientations of the primary zinc-rich crystals in the alloy were characterized using Electron Backscattered Diffraction (EBSD). The affecting mechanism of the HMFs on the alignments and orientations of the primary zinc-rich crystals was discussed briefly.

## 2. Results and Discussion

Figure 1 shows the differential scanning calorimetry (DSC) curve of the Sn-12Zn-6Bi alloy upon cooling, where two exothermic peaks are detected. This is similar to the case of the Sn-8Zn-6Bi alloy [27], according to which the reaction orders should be as follows: L → L + primary Zn → L + primary Zn + secondary Sn → primary Zn + secondary Sn + eutectic (Sn + Zn). Furthermore, as the solubility of Bi in Sn decreases with the drop in the temperature, Bi crystals will be precipitated from the Sn matrix. The small peak in the curve corresponds to the crystallization of the primary Zn in the melt.

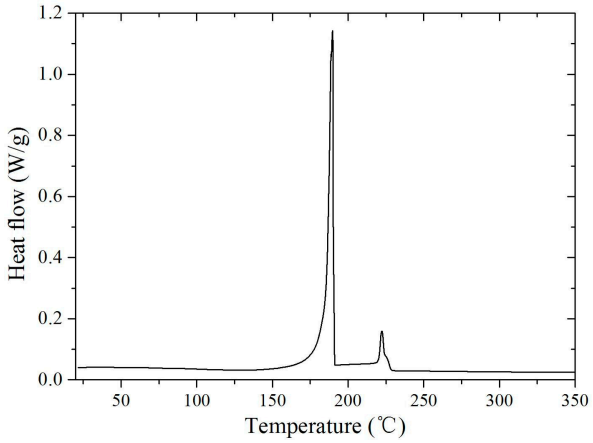


**Figure 1.** DSC curve of the ternary Sn-12Zn-6Bi alloy upon cooling.

Figure 2 shows the longitudinal macrostructures of the Sn-Zn-Bi specimens under various HMFs. As can be observed, the large dark primary zinc-rich crystals reveal a typical needle-like form. Obviously, the alignments of these primary crystals are heavily affected by the application of HMFs. Without and with a 0.6 T HMF, they are randomly aligned (Figure 2a,b). When increasing the HMF to 1.5 and 3 T, some crystals in the central regions of the specimens tend to align vertically, i.e., with the longer axis parallel to HMF direction $\boldsymbol{B}$ (Figure 2c,d). When the HMF is increased to 5 T, almost all of the crystals in the central regions align vertically. However, a further increase of the HMF to 12 T does not further enhance the alignment tendency. Moreover, it should be noted that the needle-like zinc-rich crystals in the peripheral regions are less affected by the application of the HMFs, i.e., they align randomly in all cases.

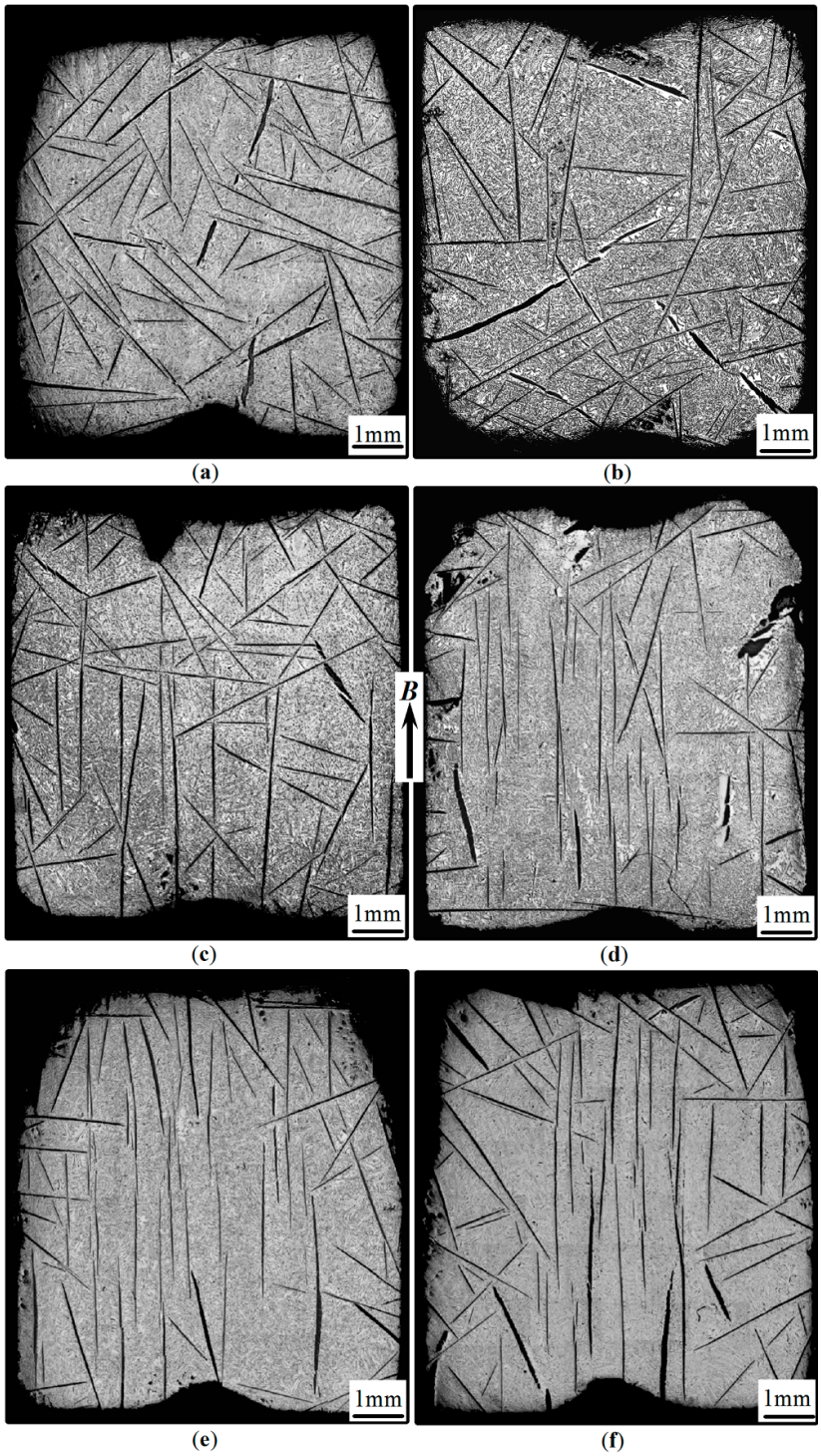


**Figure 2.** Longitudinal macrostructures of the Zn-Sn-Bi alloy under various magnetic fields: (**a**) 0 T; (**b**) 0.6 T; (**c**) 1.5 T; (**d**) 3 T; (**e**) 5 T; (**f**) 12 T. The arrow indicates the direction of ***B***.

For more details, Figure 3 shows the microstructures in the central regions of the specimens under various HMFs, in which the regular alignments of the needle-like zinc-rich crystals can be more clearly observed. Other than this, it can also be seen that many fine dark-gray fibers are distributed randomly in the white-gray matrix surrounding the large primary zinc-rich crystals. Some small medium-gray globular crystals also exist and attach to each fiber to form a string-of-pearls-like morphology, as shown in the magnified insert in Figure 3a. A microstructural analysis indicates that the dark-gray fibers,

the white-gray matrix, and the medium-gray globes are the eutectic zinc-rich phase, β-Sn matrix, and Bi crystals, respectively. Here, it should be mentioned that the various contrasts and morphologies of the eutectics are related to the polishing time: as the polishing solution is corrosive, different polishing times will result in different appearances (e.g., Figure 3b,c correspond to a longer polishing time so that many globular Bi crystals are revealed). However, it is certain that the random alignments of the fiber-like eutectic zinc-rich phase are unaffected by the HMF.

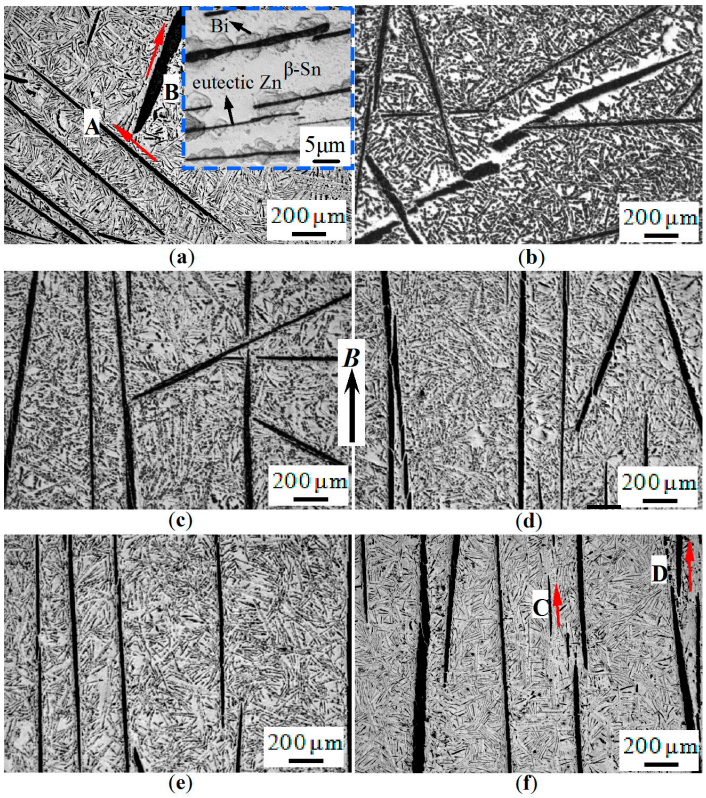


**Figure 3.** Microstructures corresponding to the central regions of the macrostructures in Figure 2: (**a**) 0, (**b**) 0.6, (**c**) 1.5, (**d**) 3, (**e**) 5, and (**f**) 8.8 T, respectively. The insert in (a) shows the magnified microstructure consisting of eutectic zinc-rich phase, β-Sn matrix, and Bi crystals, respectively. A, B, C, and D denote the crystals that will be further analyzed in Figure 6. The arrow indicates the direction of ***B***.

To further understand the effects of the HMFs, Figure 4 shows the transverse macrostructures of the specimens. As can be observed, the large primary zinc-rich crystals still reveal a needle-like form, but align randomly in all cases. However, the unchanged needle-like form indicates that the large zinc-rich crystals may be plate-shaped in three dimensions. To identify this, Figure 5a,b show the microstructures of the cubes cut from the 0 and 12 T specimens, respectively. It can be seen that the primary zinc-rich crystals in surfaces 1, 2, and 3 connect perfectly at the edges of both of the cubes, confirming a plate shape in three dimensions, irrespective of whether the HMF is applied. Nevertheless, the needle-shaped form (with sharp ends) in two dimensions suggests that the edges of these plates should have a tapered transition in thickness. Furthermore, the primary zinc-rich plates exhibit some faceted growth character, as can be seen from the relatively smooth interface traces. A crystallographic interface calculation indicates that the large surfaces of the plates correspond to the {0001} basal plane. This result can also be indirectly proven by the <0001> pole figures in Figure 6a,b, corresponding to the crystals A & B in Figure 3a and C & D in Figure 3f, respectively. The projection lines OA, OB, OC, and OD are approximately perpendicular to the interface traces of the crystals A, B, C, and D in Figure 3 (see the arrows denoting the extension directions of the interfaces), respectively.

Furthermore, it should be mentioned that crystal B in Figure 3a is coarser than the others. This is because that it approximately exposes the {0001} basal plane in the longitudinal section, as evidenced by pole A near the center point O in Figure 6a. From the analysis above, it can be concluded that the plate-shaped primary zinc-rich crystals should grow in three dimensions, as follows: spreading rapidly in the {0001} basal plane and then decreasing gradually in thickness at the edges. Figure 7 schematically shows the three-dimensional morphology of a primary zinc-rich crystal, in conjunction with the hexagonal unit cells, denoting its orientations relative to the observation plane. It should be mentioned here that the growth manner of the primary zinc-rich crystals in the present alloy is quite different from that of the crystals in Zn-Sn and Zn-Al alloys, which, as mentioned previously, grow along the <10$\bar{1}$0> and/or <0001> directions to form complex dendritic morphologies [13,14,26]. Such a growth manner may be related to the types and amounts of alloying elements, which affect the growth kinetics of zinc-rich crystals. This is open to future research.

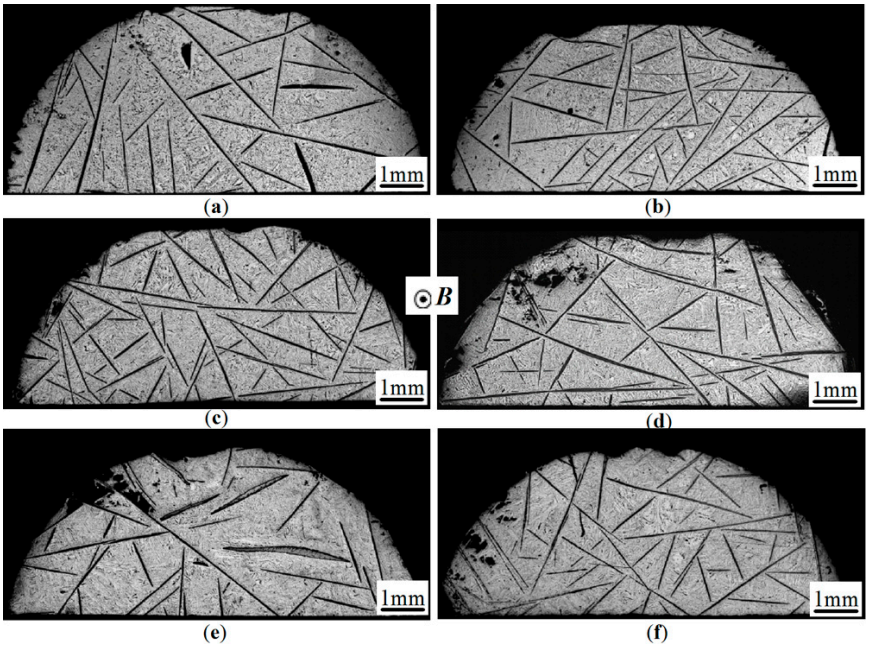


**Figure 4.** Transverse macrostructures of the specimens under various HMFs: (**a**) 0 T; (**b**) 0.6 T; (**c**) 1.5 T; (**d**) 3 T; (**e**) 5 T; (**f**) 12 T.

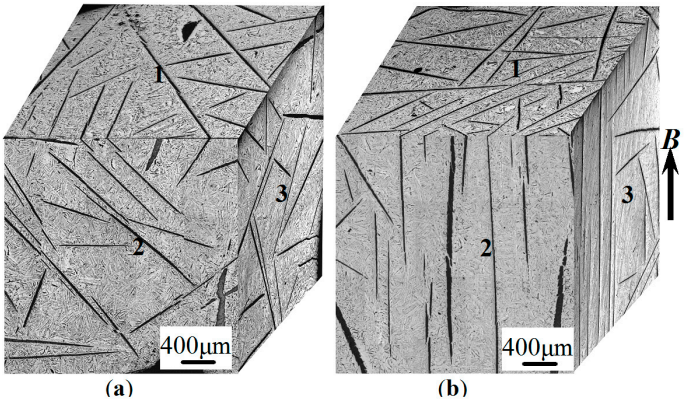


**Figure 5.** Microstructures of the cubes cut from the 0 and 12 T specimens. 1, 2, and 3 indicate the different surfaces of the cubes. The arrow indicates the direction of ***B***.

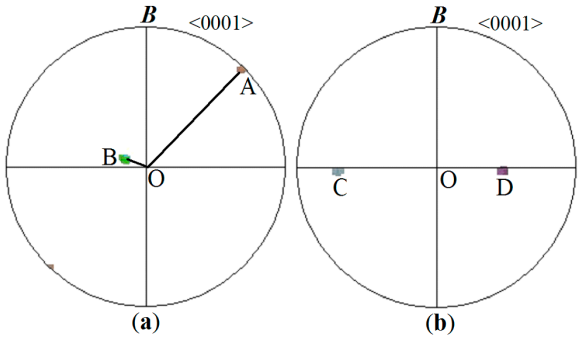


**Figure 6.** <0001> pole figures corresponding to the primary zinc-rich crystals (**a**) A & B in Figure 3a and (**b**) C & D in Figure 3f, respectively.

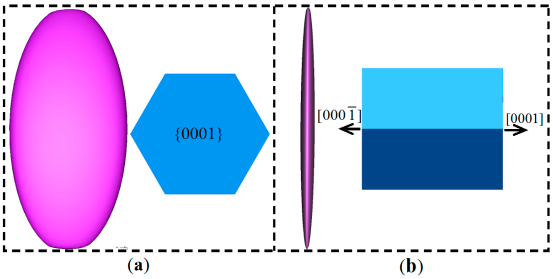


**Figure 7.** Schematic morphology of a primary zinc-rich crystal in three dimensions: (**a**) front and (**b**) side views. The hexagonal unit cells denote its orientations relative to the observation plane.

It has been optically observed that the primary zinc-rich crystals in the Sn-Zn-Bi alloy are highly aligned owing to the application of the HMFs. To discover more structural transformation information, further crystallographic analysis was conducted in this work. Figure 8a,b show the phase maps (zinc-rich crystals—red; β-Sn matrix—blue) and the all-Euler orientation micrographs corresponding to the longitudinal structures without and with a 12 T HMF, respectively. It can be seen that the large primary zinc-rich crystals are distributed in the fine β-Sn grains. Irrespective of whether the HMF is applied, the primary zinc-rich crystals show different colors, indicating that they have different orientations. However, the crystallographic calculation suggests that the HMF tends to orient its *c*-axes perpendicular to ***B***. Figure 9a,b show the scattered <0001> pole figures corresponding to the primary zinc-rich crystals in Figure 8a,b, respectively. The <0001> poles are randomly distributed in the absence of the HMF, whereas they reveal a linear distribution in the presence of the HMF. This further proves that the primary zinc-rich crystals tend to orient preferentially with the <0001> direction, i.e., the *c*-axis, perpendicular to ***B***. This orientation feature is consistent with that of the dendritic primary zinc-rich crystals under a HMF [13]. A detailed crystallographic analysis was also conducted on the β-Sn matrix, implying no preferential orientation, even with a 12 T HMF.

As analysed in other work [13], the preferential orientation of the hexagonal primary zinc-rich crystals should be related to their magnetocrystalline anisotropy. According to the magnetization energy theory, the easy magnetization axis should be parallel to the magnetic field for paramagnetic materials and perpendicular to the magnetic field for diamagnetic materials [18,28]. Zinc is a diamagnetic material with a smaller magnetic susceptibility along the *c*-axis ($-0.169\times10^{-6}$ cm$^3$/g) than that in the direction perpendicular to the *c*-axis ($0.124\times10^{-6}$ cm$^3$/g) [29]. To minimize the magnetization energy, the *c*-axis of the primary zinc-rich crystals tends to be rotated to the direction perpendicular to ***B*** under the HMFs. The driving force to start the rotation is the magnetic torque, as analysed in detail elsewhere [17,18,30]. However, to complete this rotation, a weak constraint medium is indispensable for the crystals [28]. For the present Sn-Zn-Bi alloy in this work, the zinc-rich crystals are primarily crystallized from the melt during the solidification process. The surrounding liquid

provides a free rotation environment for them. However, for the crystals in the peripheral regions of the specimens, their rotations may be hindered by the crucible walls. It is known that the melt solidifies inward from the crucible wall in a non-directional solidification way. This means that the crucible walls may act as the effective nucleation sites for the primary zinc-rich crystals, as a result of which their rotations are prevented by the crucible walls. After nucleation, these crystals grow towards the central regions of the specimens, and finally reveal random alignments in all cases.

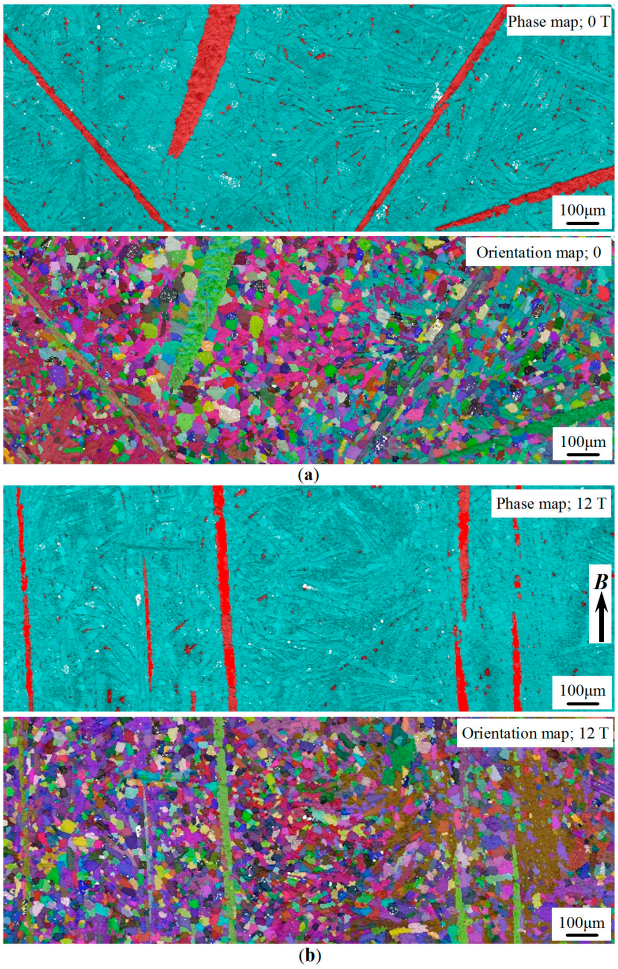


**Figure 8.** Phase maps and all-Euler orientation micrographs corresponding to the longitudinal structures (**a**) without and (**b**) with a 12 T HMF, respectively. The arrow indicates the direction of ***B***.

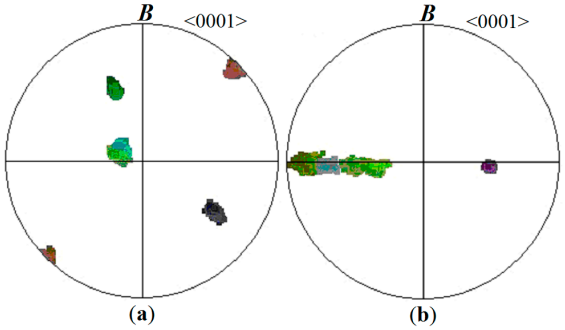


**Figure 9.** Scattered <0001> pole figures corresponding to the primary zinc-rich crystals in (**a**) Figure 8a and (**b**) in Figure 8b, respectively.

Now it can be understood that in the absence of the HMFs, all the plate-shaped primary zinc-rich crystals align randomly, as schematically shown in Figure 10a. When the HMFs are applied, the *c*-axes of the crystals in the central regions of specimens are fixed in the plane perpendicular to ***B***. As the {0001} basal plane corresponds to the large surfaces of the plate-shaped crystals, they finally exhibit a vertical alignment, as schematically shown in Figure 10b.

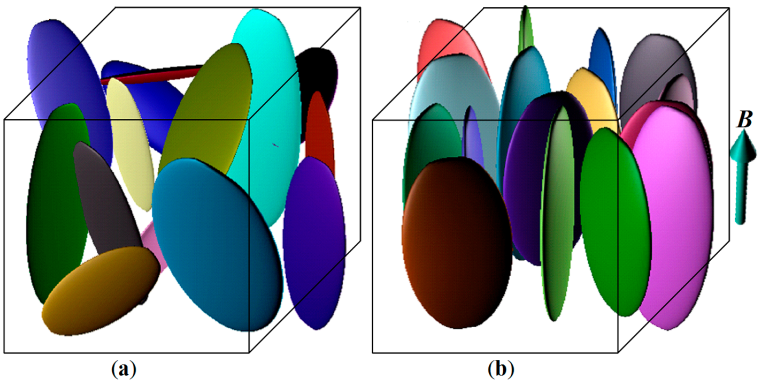


**Figure 10.** Schematic diagrams showing the alignments of the plate-shaped primary zinc-rich crystals (**a**) without and (**b**) with a HMF, respectively. The arrow in (b) indicates the direction of ***B***.

## 3. Materials and Methods

A ternary Sn-12 wt % Zn-6 wt % Bi (nominal composition) alloy was prepared by melting pure zinc (99.9 wt %), tin (99.95 wt %), and bismuth (99.9 wt %) in an induction furnace. The alloy was reheated to 673 K (400 °C) at a rate of 5 K/min in an electric resistance furnace under an argon atmosphere and held at this temperature for 25 min to ensure a homogeneous composition. Afterwards, the melt was cooled to room temperature at a rate of about 10 K/min. From the start of the reheating until the end of the cooling, different uniform-distributed HMFs were applied, as introduced in detail elsewhere [13].

The HMF-treated as-cast ingots ($\Phi$ 10 × 12 mm) were cut longitudinally or transversely (parallel or perpendicular to the HMF direction ***B***), following a standard mechanical polishing. The macro/microstructures were observed with a Leica DMR optical microscope (Leica Microsystems, Wetzlar, Germany). Moreover, two small cubes were also cut from the 0 and 12 T specimens for three-dimensional microstructure observations. After further polishing plus Ar ion beam cleaning, EBSD auto scanning was performed on the specimens for crystallographic analysis on a Zeiss ULTRA PLUS FE-SEM (Carl Zeiss, Jena, Germany), equipped with an Oxford-HKL Channel 5 system (Oxford Instruments, Abingdon, Oxfordshire, UK). Differential scanning calorimetry (DSC) was carried out on a Q100 TA Instrument (TA Instruments, Newcastle, DE, USA) to understand the cooling process of the alloy: a 20 mg specimen was cooled from 623 K (350 °C) to 293 K (20 °C) at a constant rate of 5 K/min in Ar flow.

The large faceted interface of the primary zinc-rich crystals exposed to the Sn matrix was calculated by an indirect two-trace method [31,32]. The preferential direction of the primary zinc-rich crystals relative to the HMF direction is determined as follows: first, the ***B*** vector in the sample coordinate system is transformed to its equivalent vector in the crystal coordinate system with the measured orientation data of the crystals; then, a plane is defined by the cross product of these two differently oriented vectors; finally, the statistically representative crystalline direction close to the normal vector of the plane is determined as the preferential direction [13].

## 4. Conclusions

A ternary Sn-12Zn-6Bi alloy was solidified under different HMFs, and it was found that:

a. Irrespective of whether the HMF is applied, the primary zinc-rich crystals reveal a plate-shaped form and grow in three dimensions, as follows: spreading rapidly in the {0001} basal plane and then decreasing the thickness at the edges gradually;
b. In the absence of the HMF, the plate-shaped primary zinc-rich crystals align randomly, whereas in the presence of the HMF, those in the central regions of the specimens tend to align vertically;
c. Crystallographic analyses indicate that the vertically aligned primary zinc-rich crystals orient preferentially with the *c*-axis perpendicular to ***B***;
d. The preferential orientation and thus the regular vertical alignment should be related to the magnetocrystalline anisotropy of the diamagnetic primary zinc-rich crystals.

**Acknowledgments:** The authors acknowledge the Liaoning Provincial Natural Science Foundation of China (2015021002), the Fundamental Research Funds for the Central Universities (N150904003), the China Postdoctoral Science Foundation (2015M570250), the Northeastern University Postdoctoral Science Foundation (20150202), the National Natural Science Foundation of China (51690161, 51201029, 51574075, 51374067 and 51674078), and the Science and Technology Program of Guangzhou, China (2015B090926013).

**Author Contributions:** Chunyan Ban conceived and designed the experiments; Lei Li wrote the paper; Ruixue Zhang performed the experiments; Haitao Zhang, Minghui Cai and Yubo Zuo contributed the materials; Qingfeng Zhu, Xiangjie Wang, and Jianzhong Cui conducted the data analysis.

**Conflicts of Interest:** The authors declare no conflict of interest.

## References

1. Li, L.; Zhang, Y.D.; Esling, C.; Zhao, Z.H.; Zuo, Y.B.; Zhang, H.T.; Cui, J.Z. Formation of feathery grains with the application of a static magnetic field during direct chill casting of Al-9.8 wt % Zn alloy. *J. Mater. Sci.* **2009**, *44*, 1063–1068. [CrossRef]
2. Li, L.; Zhang, Y.D.; Esling, C.; Zhao, Z.H.; Zuo, Y.B.; Zhang, H.T.; Cui, J.Z. Formation of twinned lamellas with the application of static magnetic fields during semi-continuous casting of Al-0.24 wt % Fe alloy. *J. Cryst. Growth* **2009**, *311*, 3211–3215. [CrossRef]
3. Vives, C. Effects of forced electromagnetic vibrations during the solidification of aluminum alloys: Part II. solidification in the presence of colinear variable and stationary magnetic fields. *Metall. Trans. B* **1996**, *27*, 457–464. [CrossRef]
4. Vives, C. Effects of forced electromagnetic vibrations during the solidification of aluminum alloys: Part I. solidification in the presence of crossed alternating electric fields and stationary magnetic fields. *Metall. Trans. B* **1996**, *27*, 445–455. [CrossRef]
5. Singh, R.; Thomas, B.G.; Vanka, S.P. Effects of a magnetic field on turbulent flow in the mold region of a steel caster. *Metall. Trans. B* **2013**, *44*, 1201–1221. [CrossRef]
6. Hu, S.D.; Dai, Y.C.; Gagnoud, A.; Fautrelle, Y.; Moreau, R.; Ren, Z.M.; Deng, K.; Li, C.J.; Li, X. Effect of a magnetic field on macro segregation of the primary silicon phase in hypereutectic Al-Si alloy during directional solidification. *J. Alloy. Compd.* **2017**, *722*, 108–115. [CrossRef]
7. Li, H.X.; Fautrelle, Y.; Hou, L.; Du, D.F.; Zhang, Y.K.; Ren, Z.M.; Lu, X.G.; Moreau, R.; Li, X. Effect of a weak transverse magnetic field on the morphology and orientation of directionally solidified Al–Ni alloys. *J. Cryst. Growth* **2016**, *436*, 68–75. [CrossRef]
8. Du, D.F.; Guan, G.; Gagnoud, A.; Fautrelle, Y.; Ren, Z.M.; Lu, X.G.; Wang, H.; Dai, Y.M.; Wang, Q.L.; Li, X. Effect of a high magnetic field on the growth of å-$CuZn_5$ dendrite during directionally solidified Zn-rich Zn–Cu alloys. *Mater. Charact.* **2016**, *111*, 31–42. [CrossRef]
9. Li, X.; Wang, J.; Du, D.F.; Zhang, Y.K.; Fautrelle, Y.; Nguyen-Thi, H.; Gagnoud, A.; Ren, Z.M.; Moreau, R. Effect of a transverse magnetic field on the growth of equiaxed grains during directional solidification. *Mater. Lett.* **2015**, *161*, 595–600. [CrossRef]

10. Li, L.; Zhu, Q.F.; Zhang, H.; Zuo, Y.B.; Ban, C.Y.; He, L.Z.; Liu, H.T.; Cui, J.Z. Morphological and crystallographic characterization of solidified Al–3Ti–1B master alloy under a high magnetic field. *Mater. Charact.* **2014**, *95*, 1–11. [CrossRef]
11. Xuan, W.D.; Liu, H.; Lan, J.; Li, C.J.; Zhong, Y.B.; Li, X.; Cao, G.H.; Ren, Z.M. Effect of a transverse magnetic field on stray grain formation of Ni-Based single crystal superalloy during directional solidification. *Metall. Trans. B* **2016**, *6*, 3231–3236. [CrossRef]
12. Xuan, W.D.; Liu, H.; Li, C.J.; Ren, Z.M.; Zhong, Y.B.; Li, X.; Cao, G.H. Effect of a high magnetic field on microstructures of Ni-Based single crystal superalloy during seed melt-back. *Metall. Trans. B* **2016**, *47*, 828–833. [CrossRef]
13. Li, L.; Li, Z.B.; Zhang, Y.D.; Esling, C.; Liu, H.T.; Zhao, Z.H.; Zhu, Q.F.; Zuo, Y.B.; Cui, J.Z. Crystallographic effect of a high magnetic field on hypoeutectic Zn-Al during solidification process. *J. Appl. Crystallogr.* **2014**, *47*, 606–612. [CrossRef]
14. Li, L.; Ban, C.Y.; Shi, X.C.; Zhang, H.T.; Cai, M.H.; Liu, H.T.; Cui, J.Z.; Nagaumi, H. Crystallographic growth pattern of zinc-rich plate-like cells under a high magnetic field. *Mater. Lett.* **2016**, *185*, 447–451. [CrossRef]
15. Li, L.; Zhang, Y.D.; Esling, C.; Jiang, H.X.; Zhao, Z.H.; Zuo, Y.B.; Cui, J.Z. Influence of a high magnetic field on the precipitation behaviors of the primary $Al_3Fe$ phase during the solidification of hypereutectic Al-3.31 wt % Fe alloy. *J. Cryst. Growth* **2012**, *339*, 61–69. [CrossRef]
16. Li, L.; Zhao, Z.H.; Zuo, Y.B.; Zhu, Q.F.; Cui, J.Z. Effect of a high magnetic field on the morphological and crystallographic features of primary $Al_6Mn$ phase formed during solidification process. *J. Mater. Res.* **2013**, *28*, 1567–1573. [CrossRef]
17. Li, L.; Zhang, Y.D.; Esling, C.; Qin, K.; Zhao, Z.H.; Zuo, Y.B.; Cui, J.Z. A microstructural and crystallographic investigation on the precipitation behaviour of primary $Al_3Zr$ phase under high magnetic field. *J. Appl. Crystallogr.* **2013**, *46*, 421–429. [CrossRef]
18. Wang, C.J.; Wang, Q.; Wang, Z.Y.; Li, H.T.; Nakajima, K.; He, J.C. Phase alignment and crystal orientation of $Al_3Ni$ in Al–Ni alloy by imposition of a uniform high magnetic field. *J. Cryst. Growth* **2008**, *310*, 1256–1263. [CrossRef]
19. Li, X.; Ren, Z.M.; Fautrelle, Y. The alignment, aggregation and magnetization behaviors in MnBi–Bi composites solidified under a high magnetic field. *Intermetallics* **2007**, *15*, 845–855. [CrossRef]
20. Li, X.; Ren, Z.M.; Fautrelle, Y. Effect of high magnetic fields on the microstructure in directionally solidified Bi–Mn eutectic alloy. *J. Cryst. Growth* **2007**, *299*, 41–47. [CrossRef]
21. Li, L.; Xu, B.; Tong, W.P.; He, L.Z.; Ban, C.Y.; Zhang, H.; Zuo, Y.B.; Zhu, Q.F.; Cui, J.Z. Directional growth behavior of α(Al) dendrites during concentration-gradient-controlled solidification process in static magnetic field. *Trans. Nonferrous Met. Soc. China* **2015**, *25*, 2438–2445. [CrossRef]
22. Du, D.F.; Fautrelle, Y.; Ren, Z.M.; Moreau, R.; Li, X. Effect of a high magnetic field on the growth of ternary Al-Cu-Ag alloys during directional solidification. *Acta Mater.* **2016**, *121*, 240–256. [CrossRef]
23. Li, X.; Fautrelle, Y.; Ren, Z.M. Influence of thermoelectric effects on the solid–liquid interface shape and cellular morphology in the mushy zone during the directional solidification of Al–Cu alloys under a magnetic field. *Acta Mater.* **2007**, *55*, 3803–3813. [CrossRef]
24. Rhême, M.; Gonzales, F.; Rappaz, M. Growth directions in directionally solidified Al–Zn and Zn–Al alloys near eutectic composition. *Scripta Mater.* **2008**, *59*, 440–443.
25. Haxhimali, T.; Karma, A.; Gonzales, F.; Rappaz, M. Orientation selection in dendritic evolution. *Nat. Mater.* **2006**, *5*, 660–664. [CrossRef] [PubMed]
26. Li, L.; Ban, C.Y.; Shi, X.C.; Zhang, H.T.; Zuo, Y.B.; Zhu, Q.F.; Wang, X.J.; Zhang, H.; Cui, J.Z.; Nagaumi, H. Effects of a high magnetic field on the primary zinc-rich crystals in hypoeutectic Zn-Sn alloy. *J. Cryst. Growth* **2017**, *463*, 59–66. [CrossRef]
27. Kima, Y.S.; Kim, K.S.; Hwang, C.W.; Suganuma, K. Effect of composition and cooling rate on microstructure and tensile properties of Sn–Zn–Bi alloys. *J. Alloy. Compd.* **2003**, *352*, 237–245. [CrossRef]
28. Asai, S. Crystal orientation of non-magnetic materials by imposition of a high magnetic field. *Sci. Technol. Adv. Mater.* **2003**, *4*, 455–460. [CrossRef]
29. Marcus, J.A. Magnetic Susceptibility of Zinc at Liquid Hydrogen Temperatures. *Phys. Rev.* **1949**, *76*, 413–416. [CrossRef]
30. Sugiyama, T.; Tahashi, M.; Sassa, K.; Asai, S. The control of crystal orientation in non-magnetic metals by imposition of a high magnetic field. *ISIJ. Int.* **2003**, *43*, 855–861. [CrossRef]

31. Zhang, Y.D.; Esling, C.; Zhao, X.; Zuo, L. Indirect two-trace method to determine a faceted low-energy interface between two crystallographically correlated crystals. *J. Appl. Cryst.* **2007**, *40*, 436–440. [CrossRef]
32. Li, L.; Zhang, Y.D.; Esling, C.; Jiang, H.; Zhao, Z.H.; Zuo, Y.B.; Cui, J.Z. Crystallographic features of primary $Al_3Zr$ phase. *J. Cryst. Growth* **2011**, *316*, 172–176. [CrossRef]

© 2017 by the authors. Licensee MDPI, Basel, Switzerland. This article is an open access article distributed under the terms and conditions of the Creative Commons Attribution (CC BY) license (http://creativecommons.org/licenses/by/4.0/).